Charge ordering in $CaCu_xMn_{7-x}O_{12}$ (x = 0.0 and 0.1) compounds

2008 J. Phys.: Condens. Matter 20 104239

(http://iopscience.iop.org/0953-8984/20/10/104239)

J. Phys.: Condens. Matter **20** (2008) 104239 (7pp) doi:10.1088/0953-8984/20/10/104239

Charge ordering in $CaCu_xMn_{7-x}O_{12}$ ($x = 0.0$ and 0.1) compounds

W Sławiński[1], R Przeniosło[1], I Sosnowska[1], M Bieringer[2], I Margiolaki[3], A N Fitch[3] and E Suard[4]

[1] Institute of Experimental Physics, University of Warsaw, Hoża 69, PL-00 681 Warsaw, Poland
[2] Department of Chemistry, University of Manitoba, Winnipeg, R3T 2N2, Canada
[3] European Synchrotron Radiation Facility, BP220, Grenoble Cedex, F-38043, France
[4] Institut Laue-Langevin, 6 rue Jules Horowitz, BP 156X F-38042 Grenoble, France

Received 13 July 2007, in final form 15 October 2007
Published 19 February 2008
Online at stacks.iop.org/JPhysCM/20/104239

Abstract

The crystal structure of $CaMn_7O_{12}$ and $CaCu_{0.1}Mn_{6.9}O_{12}$ has been studied by synchrotron radiation (SR) based powder x-ray diffraction and neutron powder diffraction in the temperature range from 10 K up to 290 K. The lattice parameter a exhibits a minimum at 45 K in $CaMn_7O_{12}$. The c lattice parameter in $CaMn_7O_{12}$ and $CaCu_{0.1}Mn_{6.9}O_{12}$ has a maximum at the same temperature. Additional Bragg peaks have been found in the SR diffraction patterns in $CaMn_7O_{12}$ and $CaCu_{0.1}Mn_{6.9}O_{12}$ below 250 K and 220 K, respectively. All diffraction peaks have been indexed as $(h, k, l \pm \kappa)$, where κ was equal to 0.079(15) for $CaMn_7O_{12}$ and 0.093(15) for $CaCu_{0.1}Mn_{6.9}O_{12}$. The incommensurate low-temperature diffraction peaks are not observed in neutron diffraction patterns. This leads to the conclusion that the phase transition to the incommensurate structure is due to charge ordering rather than atomic position modulation. The charge ordering temperature coincides with dielectric constant changes of four orders of magnitude for $CaMn_7O_{12}$.

1. Introduction

Among the diverse group of manganese oxides, the $CaCu_xMn_{7-x}O_{12}$ family is particularly intriguing. This group of materials has been widely studied because of the dependence of its physical properties on the Cu concentration, x. The complex phase diagram was described in [1], where semiconducting, ferrimagnetic, metallic and paramagnetic phases were found for several compounds with $0 \leqslant x \leqslant 3$. $CaCu_xMn_{7-x}O_{12}$ compounds show colossal magnetoresistance with negative magnetoresistivities of MR $= -40\%$ for $x = 3$ [2] and MR $= -65\%$ for $x = 1.0$ [3]. It has been shown for $CaCu_xMn_{7-x}O_{12}$ with low Cu content ($x \leqslant 0.2$) that there is a low-temperature trigonal phase and a high-temperature cubic phase [4, 5]. Furthermore, phase separation has been observed in undoped ($x = 0$) [4] and doped ($x = 0.1$ and 0.2) [5] samples. The coexisting large crystalline domains for both phases have been reported for a 40 K temperature interval using SR diffraction. The observation of phase separation in $CaMn_7O_{12}$ has been confirmed recently by ^{57}Fe Mössbauer studies of $CaMn_{6.97}Fe_{0.03}O_{12}$ [6]. $CaMn_7O_{12}$ shows a colossal dielectric constant of about $\epsilon = 10^6$ at room temperature (RT) [7]. The value of ϵ drops down to about 10^2 between 250 and 150 K [7]. Our previous SR diffraction studies of $CaMn_7O_{12}$ have shown charge modulation below 250 K with the modulation vector $(0, 0, \kappa)$ with $\kappa = 0.07(1)$ [8]. Here we report low-temperature powder diffraction studies with highly crystalline $CaCu_xMn_{7-x}O_{12}$ samples prepared with an alternative synthetic method than previously reported samples [4, 8, 9]. The main motivation of our studies was to describe the charge modulation observed below 250 K, as described previously in [8].

1.1. Crystal structure

In the temperature range from 10 K up to 290 K the crystal structure of $CaCu_xMn_{7-x}O_{12}$ ($0 \leqslant x \leqslant 0.1$) is trigonal and can be described with the space group $R\bar{3}$. We describe the structure in the hexagonal setting with the following atomic positions: Ca^{2+} (3a), Mn^{3+}/Cu^{2+} (9a), Mn^{3+}/Mn^{4+} (9d), Mn^{4+} (3b) and O^{2-} in (18f). The lattice constants at RT are $a = 10.457\,99(2)$ Å and $b = 6.341\,98(1)$ Å in $CaMn_7O_{12}$. The important structural feature is that Mn^{3+} and Mn^{4+} ions are separated in different crystallographic positions. The central Mn^{4+} ion is octahedrally coordinated by six O^{2-}.

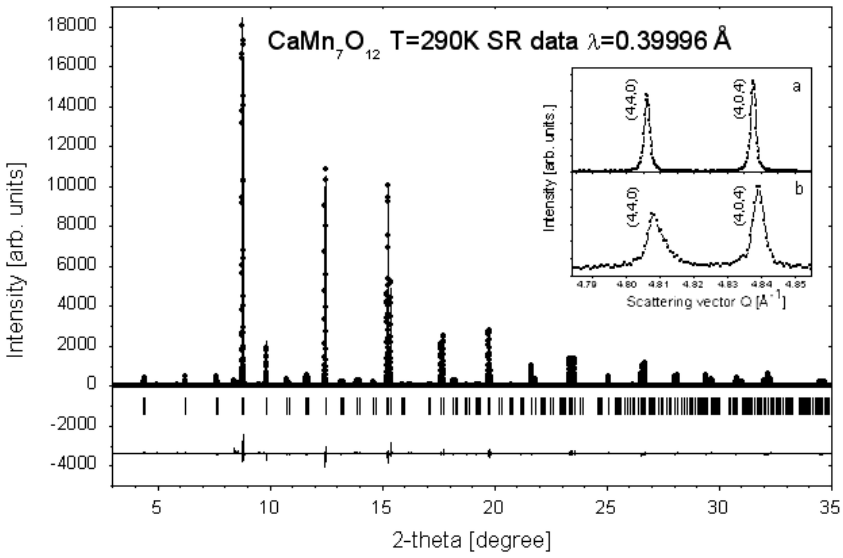

Figure 1. Rietveld plot of the SR powder diffraction pattern of $CaMn_7O_{12}$ measured at 290 K: solid circles = experimental data; solid line = calculated diffraction pattern; solid line below = difference curve. The tick marks indicate the Bragg positions for the $CaMn_7O_{12}$ phase. Parts of SR diffraction patterns of $CaMn_7O_{12}$ observed at RT for the present sample (inset a) and earlier studies published in [8] (inset b). Note the sharpened peaks for the current sample.

2. Experimental details

2.1. Measurements

Samples used in the experiments were prepared by annealing stoichiometric amounts of $CaCO_3$ (CERAC, 99.995%), CuO (CERAC, 99.999%) and Mn_2O_3 (CERAC, 99.99%) using KCl as a mineralizer. The synthesis details are described in [5].

Two sets of experiments were performed by using synchrotron radiation and neutron powder diffraction. Synchrotron radiation powder diffraction measurements were performed by using the beamline ID31 at the European Synchrotron Radiation Facility (ESRF) in Grenoble [10]. The wavelength that was used was 0.399 96 Å. The sample was placed in a 0.5 mm glass capillary which rotated during the experiments. Measurements were performed for temperatures from 10 K up to 290 K in several temperature steps. In this temperature range, a liquid-helium-cooled cryostat was used. The angular range covered by the experiment was $3.0° \leqslant 2\theta \leqslant 47.9°$, where 2θ is the scattering angle. The range of the scattering vector Q in the experiment was $0.83\ \text{Å}^{-1} \leqslant Q \leqslant 12.7\ \text{Å}^{-1}$ and $Q = \frac{4\pi}{\lambda}\sin\theta$.

Neutron powder diffraction measurements of $CaMn_7O_{12}$ and $CaCu_{0.1}Mn_{6.9}O_{12}$ were performed by using the D20 diffractometer at the Institut Laue Langevin (ILL) Grenoble with a wavelength equal to 2.421 Å. The powder sample was placed in a 8 mm diameter cylindrical vanadium container and placed in a standard orange cryostat. Diffraction patterns were measured from 10 K up to 290 K. The range of scattering vector Q in the experiment was $0.7\ \text{Å}^{-1} \leqslant Q \leqslant 4.5\ \text{Å}^{-1}$. We used the high-intensity diffractometer D20 in order to search for weak diffraction peaks with good statistical accuracy.

All powder diffraction patterns were analyzed by the Rietveld method [11] implemented in the program FullProf [12]. The space group $R\bar{3}$ was used and all atomic positions were refined as well as individual isotropic Debye–Waller factors for each kind of atom. Small amounts of $CaMn_4O_8$ [13] and Mn_2O_3 [14] impurities were identified in the samples.

3. Results

3.1. Crystal structure of $CaMn_7O_{12}$ and $CaCu_xMn_{7-x}O_{12}$

In order to visualize the diffraction data quality, the results of the Rietveld refinements of the SR diffraction pattern of $CaMn_7O_{12}$ at RT are shown in figure 1. The (4, 0, 4) and (4, 4, 0) diffraction peaks of the present $CaMn_7O_{12}$ sample (figure 1, inset (a)) and the previous $CaMn_7O_{12}$ sample [4] (figure 1, inset (b)) clearly show the significantly sharper Bragg peaks measured in this study. In our earlier studies we have used polycrystalline $CaCu_xMn_{7-x}O_{12}$ samples prepared without using a mineralizer [4, 9]. The superior crystallinities of the present samples are more suitable for studying changes in the crystal structures as well as phase separation and charge ordering transitions.

Crystal structure refinements were performed with the Rietveld method [11] using FullProf [12]. Good agreement of the refinement of an average crystal structure was reached. All structural parameters: lattice constants, atomic positions and isotropic Debye–Waller factors were refined. All atomic position parameters are in agreement with earlier studies [8]. The crystal structures of undoped $CaMn_7O_{12}$ and Cu-doped $CaCu_{0.1}Mn_{6.9}O_{12}$ are similar to each other [5].

Figure 2 presents refined values of lattice parameters a and c for $CaMn_7O_{12}$ (panels a, b) and $CaCu_{0.1}Mn_{6.9}O_{12}$ samples (panels e, f). The pseudo-cubic α_c angle defined as $\cos\alpha_c = \frac{1-\frac{3}{8}(a_h/c_h)^2}{1+\frac{3}{4}(a_h/c_h)^2}$ (panels c, g) and the unit cell volume V (panels d, h) are shown for $CaMn_7O_{12}$ and $CaCu_{0.1}Mn_{6.9}O_{12}$, respectively. The temperature dependences of the lattice parameters for

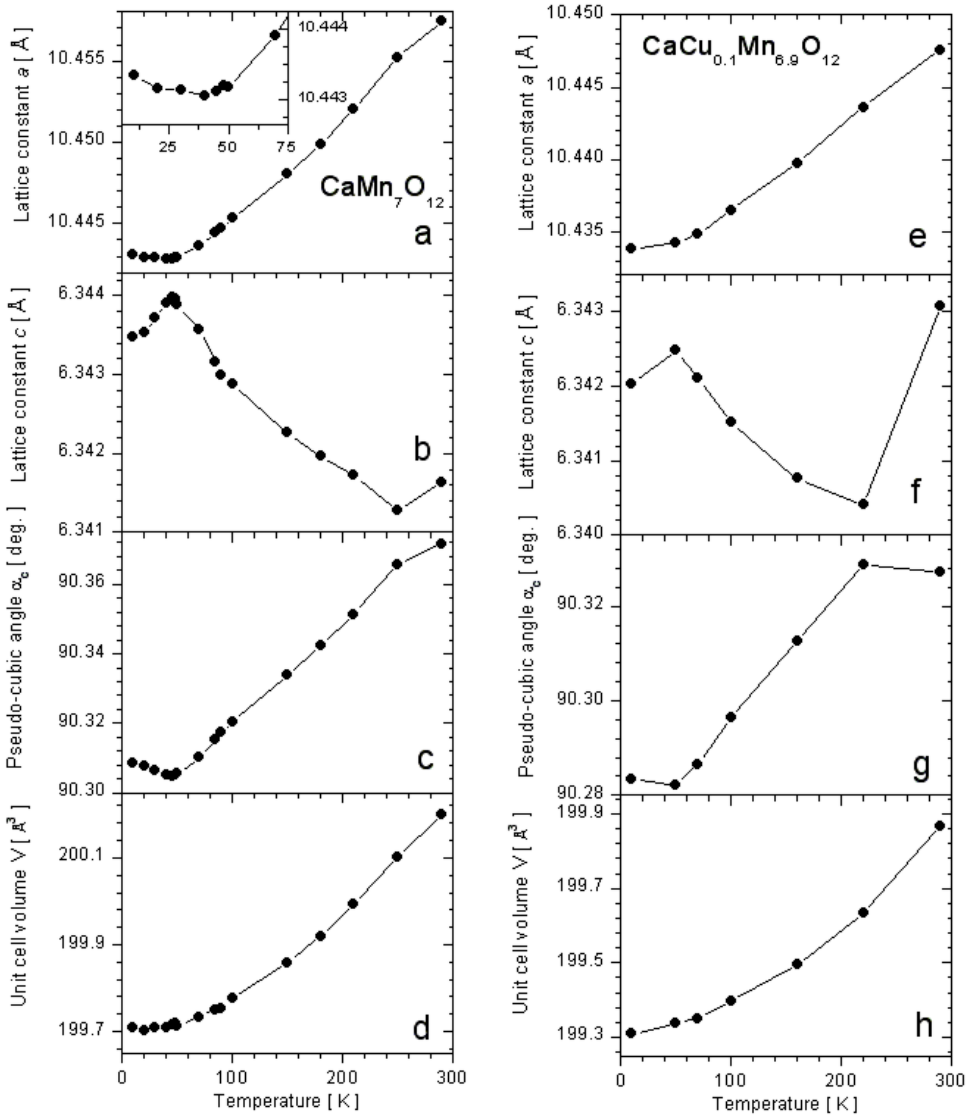

Figure 2. Temperature dependence of the lattice constant a, c, pseudo-cubic angle α_c and unit cell volume V of $CaMn_7O_{12}$ (panel a, b, c and d) and $CaCu_{0.1}Mn_{6.9}O_{12}$ (panel e, f, g and h) determined from Rietveld refinements from SR powder diffraction between 10 and 290 K. The inset in (a) shows the enlarged region from 10 to 70 K with the minimum of the lattice parameter a.

$CaMn_7O_{12}$ (figure 2) are similar to our previous results with $CaMn_7O_{12}$ [8]. There are some minor discrepancies in the lattice parameter values, probably due to systematic errors associated with the Bragg peak asymmetries.

The lattice parameters presented in this work provide more details regarding the structural changes as a function of the temperature. In the case of $CaMn_7O_{12}$, the lattice parameters a and c show a minimum and a maximum near 40 K, respectively. As a consequence, the pseudo-cubic angle α_c also shows a minimum near 40 K (figure 2(c)). The temperature-dependent lattice parameter evolution of $CaCu_{0.1}Mn_{6.9}O_{12}$ is similar, with a maximum of c at 40 K, but no explicit minimum of the a lattice constant was found. However, a change in slope of the a parameter evolution at 40 K is evident. A similar trend in the pseudo-cubic α_c angle was found. With $x = 0.1$, both lattice constants a and c are smaller than for $x = 0.0$, and this leads to a smaller unit cell volume V. A similar trend in the pseudo-cubic α_c angle with a minimum near 50 K was found.

3.2. Additional Bragg peaks observed for $CaMn_7O_{12}$ and $CaCu_{0.1}Mn_{6.9}O_{12}$

At temperatures below 250 K for $CaMn_7O_{12}$ and 220 K for $CaCu_{0.1}Mn_{6.9}O_{12}$, additional diffraction peaks have been found in the SR diffraction patterns. Note that the appearance of the additional diffraction peaks in the SR data are accompanied by minima in the hexagonal c axes parameters (figure 2). The previously reported high-temperature diffraction data for $CaCu_{0.1}Mn_{6.9}O_{12}$ confirm the c unit cell parameter minimum at 220 K [5]. At $T = 10$ K there are at least 32 and 13 additional diffraction peaks in the SR diffractograms of $CaMn_7O_{12}$ (see table 1) and $CaCu_{0.1}Mn_{6.9}O_{12}$ (see table 2), respectively. While warming up the samples, the peak intensities decrease and disappear below 250 K and 220 K in $CaMn_7O_{12}$ and $CaCu_{0.1}Mn_{6.9}O_{12}$, respectively. We were able to index all additional peaks as $(h, k, l \pm \kappa)$, where $\kappa \approx 0.079(15)$ and $\kappa \approx 0.093(15)$ for $CaMn_7O_{12}$ and $CaCu_{0.1}Mn_{6.9}O_{12}$, respectively. In our

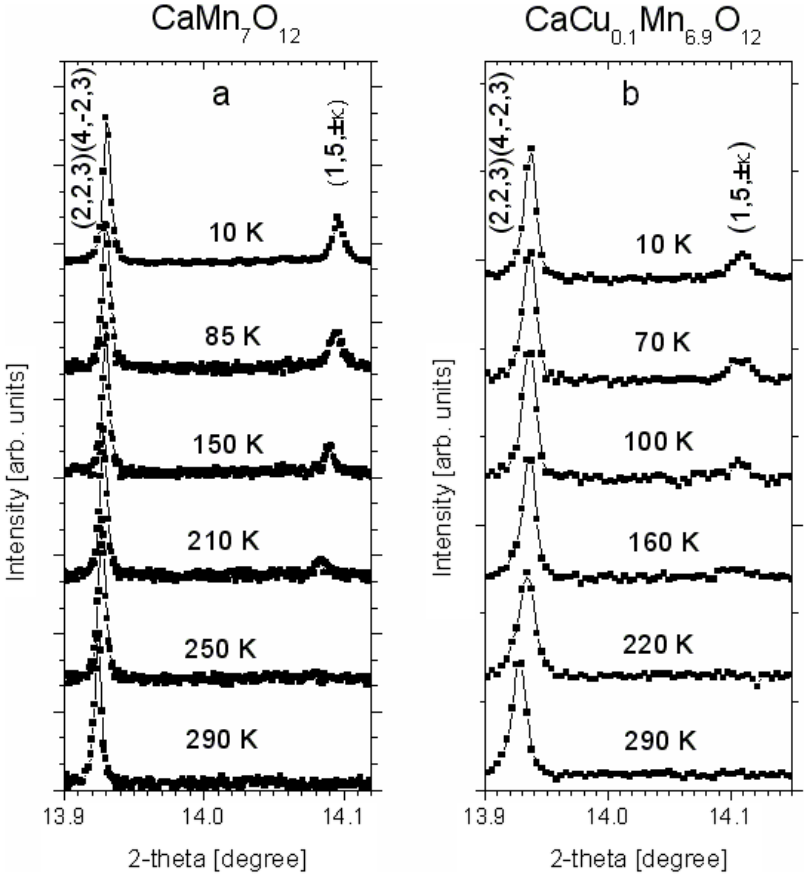

Figure 3. Parts of SR diffraction patterns of $CaMn_7O_{12}$ (left panel) and $CaCu_{0.1}Mn_{6.9}O_{12}$ (right panel) observed between 10 K and RT. The left-hand diffraction maximum is due to fundamental structural Bragg peaks (2, 2, 3)(4, −2, 3); the disappearing additional maximum on the right is indexed as (1, 5, ±κ).

Table 1. Miller indices h, k, l, modulation parameter κ and integrated intensities of the maxima for $CaMn_7O_{12}$ measured at 10 K. All additional structure maxima are indexed as $(h, k, l + \kappa)$ or $(h, k, l - \kappa)$.

h	k	l	κ	Intensity	h	k	l	κ	Intensity
1	1	1	−0.079	1.77	6	1	1	+0.079	0.98
1	2	0	±0.080	5.17	7	0	0	±0.068	2.12
1	1	2	+0.079	1.18	1	6	2	−0.079	1.47
1	3	0	±0.083	5.40	3	5	2	−0.079	2.41
2	2	1	−0.079	0.93	4	5	0	±0.075	0.53
2	1	2	−0.079	1.64	1	7	2	+0.079	4.31
1	3	2	−0.079	5.22	2	7	0	±0.100	0.25
3	3	1	−0.079	0.66	3	6	2	+0.079	1.47
1	4	2	+0.079	3.45	1	8	0	±0.064	0.57
1	5	0	±0.082	4.44	3	7	0	±0.078	2.92
0	5	2	−0.079	1.37	8	1	2	−0.080	0.96
3	3	2	+0.079	6.40	0	7	4	+0.078	1.64
3	4	0	±0.086	0.35	7	3	2	−0.079	1.58
5	1	2	−0.079	7.54	1	7	4	−0.080	13.40
1	6	0	±0.080	3.45	1	9	0	±0.073	2.50
4	3	2	−0.079	0.91	3	8	0	±0.076	1.15

Table 2. Miller indices h, k, l, modulation parameter κ and integrated intensities of the maxima for $CaCu_{0.1}Mn_{6.9}O_{12}$ measured at 10 K. All additional structure maxima are indexed as $(h, k, l + \kappa)$ or $(h, k, l - \kappa)$.

h	k	l	κ	Intensity	h	k	l	κ	Intensity
1	2	0	±0.095	4.76	0	0	5	−0.084	1.90
1	3	0	±0.095	3.57	1	6	2	−0.091	1.37
1	3	2	−0.093	9.62	3	5	2	−0.092	1.62
1	5	0	±0.094	4.41	4	4	4	−0.090	2.82
5	1	2	−0.093	5.88	0	7	4	+0.095	2.39
1	6	0	±0.096	2.88	1	7	4	+0.092	2.35
4	3	2	−0.091	3.41					

indexing scheme, all possible hexagonal (h, k, l) indices were considered; both symmetry allowed and forbidden in the trigonal space group $R\bar{3}$. Figure 3 shows parts of the diffraction patterns for $CaMn_7O_{12}$ (panel a) and $CaCu_{0.1}Mn_{6.9}O_{12}$ (panel b) measured at several temperatures in the same angular range. The intense (2, 2, 3)(4, −2, 3) Bragg reflections are due to the trigonal crystal structure, whereas the (1, 5, ±κ) maxima are due to some additional ordering at low temperatures. It is important to note that the additional (1, 5, ±κ) peaks are broader than the structural (2, 2, 3)(4, −2, 3) Bragg peaks both in $CaMn_7O_{12}$ and $CaCu_{0.1}Mn_{6.9}O_{12}$. The values of full width at half maximum (FWHM) observed in $CaMn_7O_{12}$ are 0.010° and 0.006° for the additional and fundamental Bragg peaks, respectively. The FWHMs observed in $CaCu_{0.1}Mn_{6.9}O_{12}$ are 0.020° and 0.013° for the additional and fundamental Bragg peaks, respectively.

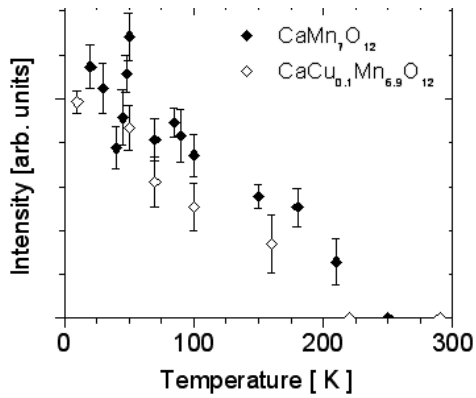

Figure 4. Temperature dependence of the intensity of the structure modulation maxima $(1, 5, \pm\kappa)$ as a function of temperature in $CaMn_7O_{12}$ (solid symbols) and $CaCu_{0.1}Mn_{6.9}O_{12}$ (open symbols), normalized to the strongest diffraction peak (2, 2, 0).

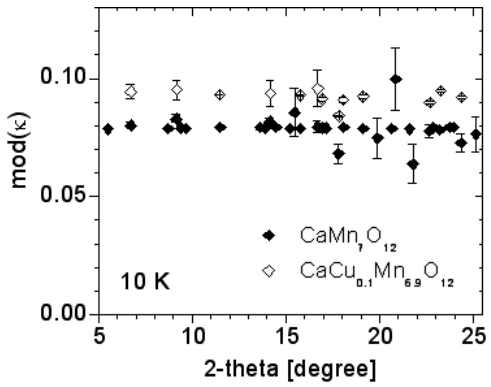

Figure 5. Angular dependence of the modulus of the modulation vector κ for $CaMn_7O_{12}$ (solid symbols) and $CaCu_{0.1}Mn_{6.9}O_{12}$ (open symbols) at 10 K.

The $(1, 5, \pm\kappa)$ maximum is the most intense at 10 K and its intensity decreases with temperature, as shown in figure 4 for $CaMn_7O_{12}$ (solid symbols) and $CaCu_{0.1}Mn_{6.9}O_{12}$ (open symbols). The intensity was normalized to the intensity of the strongest structural (2, 2, 0) diffraction peak. The temperature dependence of the $(1, 5, \pm\kappa)$ intensity is similar for both samples, but in the case of $CaCu_{0.1}Mn_{6.9}O_{12}$ the intensity values are slightly smaller. The temperatures above which no additional peaks are observed are approximately 250 K for $CaMn_7O_{12}$ and 220 K for $CaCu_{0.1}Mn_{6.9}O_{12}$, respectively. This behavior is common for all the incommensurate peaks.

The validity of our indexing scheme is supported by the narrow distribution of κ values for all incommensurate reflections, as shown in figure 5 and documented in tables 1 and 2. All the observed additional maxima are indexed as $(h, k, l\pm\kappa)$, giving a constant value of κ equal to 0.079(15) and 0.093(15) for $CaMn_7O_{12}$ (32 reflections) and $CaCu_{0.1}Mn_{6.9}O_{12}$ (13 reflections), respectively.

3.3. Comparison between SR and neutron diffraction pattern

Figure 6 shows the $CaCu_{0.1}Mn_{6.9}O_{12}$ SR diffraction pattern collected at $T = 100$ K (panel a) and the neutron diffraction

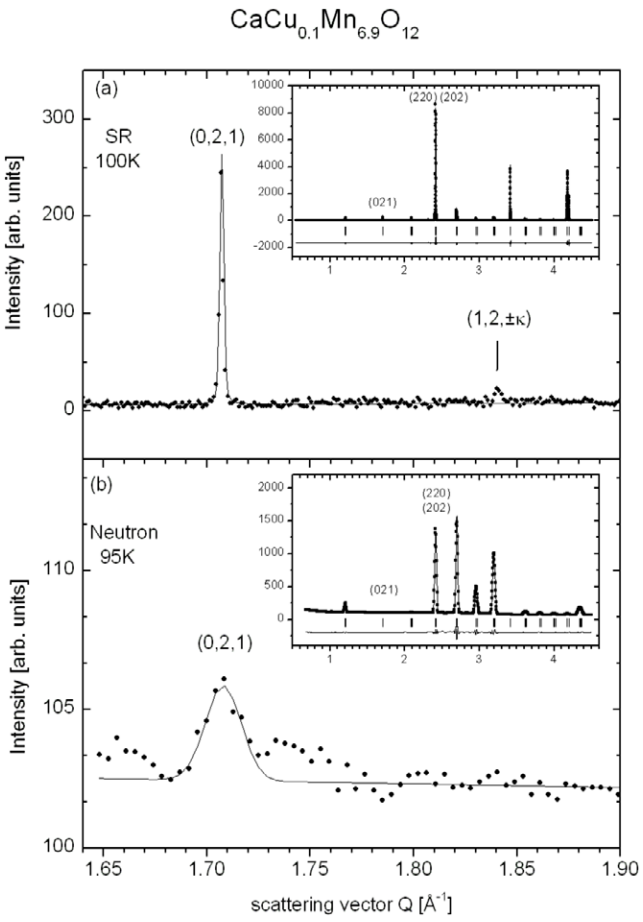

Figure 6. SR and neutron diffraction patterns of $CaCu_{0.1}Mn_{6.9}O_{12}$ presented on a common Q-scale. The main images show the same part of the observed SR diffraction pattern (at 100 K—panel (a)) and the observed neutron diffraction pattern (at 95 K—panel (b)). The region includes the commensurate (0, 2, 1) and the incommensurate $(1, 2, \pm\kappa)$ peak positions. The insets show the corresponding Rietveld plots of the SR (a) and neutron (b) powder diffraction patterns of $CaCu_{0.1}Mn_{6.9}O_{12}$ for a wider Q-range. Solid circles = experimental data; solid line = calculated diffraction pattern; solid line below = difference curve. The tick marks indicate the commensurate Bragg positions for the $CaCu_{0.1}Mn_{6.9}O_{12}$ phase.

pattern measured at 95 K (panel b). From previous magnetic ordering studies of $CaMn_7O_{12}$ [9] and $CaCu_{0.38}Mn_{6.62}O_{12}$ [15] it can be concluded that both $CaMn_7O_{12}$ and $CaCu_{0.1}Mn_{6.9}O_{12}$ are in a paramagnetic phase at 95 K and that the neutron diffraction pattern shows no magnetic Bragg peaks. In order to show the data quality we present the results of Rietveld refinement (using the commensurate structure derived from room-temperature studies [5]) of both SR and neutron diffraction patterns of $CaCu_{0.1}Mn_{6.9}O_{12}$ in the insets of figures 6(a) and (b), respectively. The incommensurate peak indexed as $(1, 2, \pm\kappa)$ is observed near $Q = 1.84$ Å^{-1} in the SR diffraction pattern. This peak is not observed in the neutron diffraction pattern. In order to compare the statistical accuracy of both diffraction patterns we can compare the intensity of weak reflections to the sum of the intensities of Bragg peaks $I(220) + I(202)$. The (2, 2, 0) and (2, 0, 2) peaks are chosen because they belong to the most intense Bragg peaks both in SR

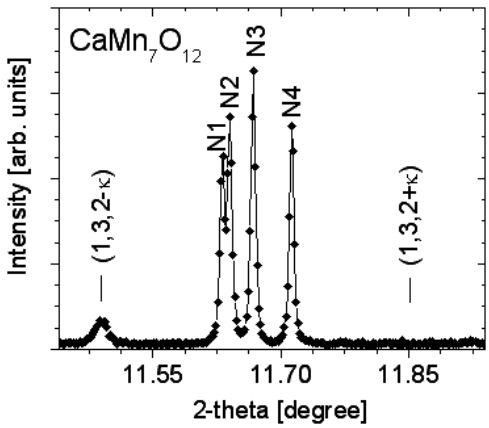

Figure 7. Part of the SR diffraction pattern of $CaMn_7O_{12}$ observed at 10 K showing $(1, 3, 2-\kappa)$ structure modulation maxima (peak present), the group of structure diffraction maxima N1 $(1, 4, 0)(4, 1, 0)$, N2 $(3, 2, 1)(5, -2, 1)$, N3 $(3, 1, 2)(4, -1, 2)$, N4 $(1, 1, 3)(2, -1, 3)$, and the calculated but absent $(1, 3, 2+\kappa)$ structure modulation peak position.

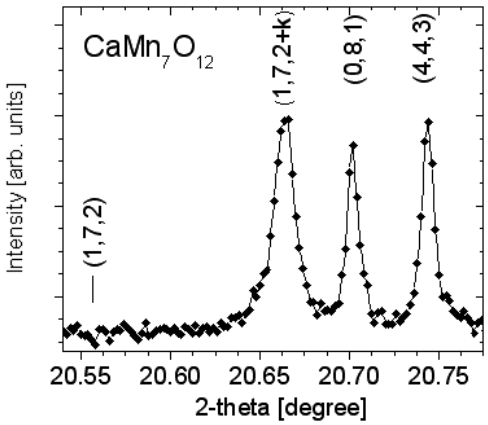

Figure 8. Selected area of SR diffraction pattern observed at 10 K with the $(1, 7, 2+\kappa)$ structure modulation maxima (present) and symmetry forbidden (1, 7, 2) position (calculated) in space group $R\bar{3}$ (absent).

(figure 6(a)) and neutron (figure 6(b)) diffraction patterns. The incommensurate $(1, 2, \pm\kappa)$ peak intensity is about 820 times smaller than the $I(220) + I(202)$ intensity (SR pattern). In the neutron diffraction pattern, the weak Bragg peak (0, 2, 1) is about 850 times smaller than the $I(220) + I(202)$ intensity. Therefore, we can conclude that the statistical accuracy of both SR and neutron patterns is similar, and one can observe weak reflections down to about $1/1000$ of the $I(220) + I(202)$ intensity. If the incommensurate reflections were of the same order of magnitude in both the SR and neutron diffraction patterns, then we could detect them using both techniques. However, it is important to note that the incommensurate maxima were not observed in the neutron diffraction patterns of $CaMn_7O_{12}$ or $CaCu_{0.1}Mn_{6.9}O_{12}$.

4. Discussion

The main question arising from our studies is concerned with the character of the low-temperature ordering, leading to the additional diffraction maxima. The absence of additional maxima in the neutron diffraction patterns indicate that the possibility of strain-type modulations associated with positional atomic displacements is negligibly small. The additional Bragg maxima observed in the SR diffraction patterns are probably due to variations in the ionic charges in the crystal lattice.

The additional Bragg maxima indexed with $l = 0$, i.e. $(h, k, \pm\kappa)$, are merged together in the powder diffraction patterns. One might therefore assume that they could be due to a modulation with the propagation vector $(0, 0, \kappa)$. This simple interpretation is not correct, because all additional Bragg maxima with $l \neq 0$ obey the following rules:

(i) when $(h, k, l-\kappa)$ is present, then $(h, k, l+\kappa)$ is absent;
(ii) when $(h, k, l+\kappa)$ is present, then $(h, k, l-\kappa)$ is absent.

The lack of both satellite maxima with $+\kappa$ and $-\kappa$ rules out the possibility of a simple charge modulation with a single propagation vector. In some cases, $(h, k, l+\kappa)$ or $(h, k, l-\kappa)$ are observed for the (h, k, l) Bragg peak, which is allowed in the space group $R\bar{3}$, as shown, for example, in figure 7. In other cases, (h, k, l) may be forbidden in the space group $R\bar{3}$, as shown, for example, in figure 8.

The dielectric properties are probably associated with some unusual charge distribution. This argument is supported by the onset temperature of the incommensurate peaks and the c-axis parameter minimum in the same temperature range as the drastic decrease in the dielectric constant ϵ, namely between 250 and 150 K for $CaMn_7O_{12}$ [7]. This strongly supports that these incommensurate peaks are due to charge ordering, and that the charge-ordered state might be the origin of the decreases in the dielectric constant. Currently, we have no structural model for the charge-ordered state consistent with all incommensurate diffraction peaks observed in SR diffraction patterns. A search for a suitable model is planned in the future.

Acknowledgments

Thanks are due to A Palewicz (University of Warsaw) for help during the measurements.

This work was partially supported by the Ministry of Sciences and Higher Education (Poland). We acknowledge the access to the ESRF (155/ESR/2006/03) and ILL facilities supported by the Ministry of Science and Higher Education (Poland). MB acknowledges the financial support from the Natural Sciences and Engineering Research Council (NSERC) of Canada, the Canada Foundation for Innovation (CFI), the Manitoba Research Innovation Fund, and the University of Manitoba.

References

[1] Zeng Z, Greenblatt M, Sunstrom J E, Croft M and Khalid S 1999 *J. Solid State Chem.* **147** 185
[2] Zeng Z, Greenblatt M, Subramanian M A and Croft M 1999 *Phys. Rev. Lett.* **82** 3164
[3] Itkis D M, Goodilin E A, Pomerantseva E A, Lobanov M V, Greenblatt M, Sivov R, Noudem J G and Tretyakov Y D 2004 *Mendeleev Commun.* **14** 153

[4] Przeniosło R, Sosnowska I, Suard E, Hewat A and Fitch A N 2002 *J. Phys.: Condens. Matter* **14** 5747
[5] Sławiński W, Przeniosło R, Sosnowska I, Bieringer M, Margiolaki M, Fitch A N and Suard E 2006 *J. Solid State Chem.* **179** 2443
[6] Presniakov I A, Rusakov V S, Gubaidulina T V, Sobolev A V, Baranov A V, Demazeau G, Volkova O S, Cherepanov V M and Goodilin E A 2007 *Solid State Commun.* **142** 509
[7] Castro-Couceiro A, Yáñez-Vilar S, Rivas-Murias B, Fondado A, Mira J, Rivas J and Señarís-Rodríguez M A 2006 *J. Phys.: Condens. Matter* **18** 3803
[8] Przeniosło R, Sosnowska I, Suard E, Hewat A and Fitch A N 2004 *Physica* B **344** 358
[9] Przeniosło R, Sosnowska I, Hohlwein D, Hauss T and Troyanchuk I O 1999 *Solid State Commun.* **111** 687
[10] Fitch A N 2004 *J. Res. Natl Inst. Stand. Technol.* **109** 133
[11] Rietveld H M 1969 *J. Appl. Crystallogr.* **2** 65
[12] Rodriguez-Carvajal J 1993 *Physica* B **192** 55
[13] Barrier N, Michel C, Maignan A, Hervieu M and Raveau B 2005 *J. Mater. Chem.* **15** 386
[14] Geller S 1971 *Acta Crystallogr.* B **27** 821
[15] Przeniosło R, Regulski M, Sosnowska I and Schneider R 2002 *J. Phys.: Condens. Matter* **14** 1061